Nonlinear Analysis of Thin Fracture Specimens Using Solid, Isoparametric Finite Elements

CARLOS G. MATOS and ROBERT H. DODDS, JR.

Department of Civil Engineering, University of Illinois, Urbana, IL 61801 USA

Abstract–This report examines the performance of various "solid" finite elements for the analysis of thin shell structures often encountered in nonlinear fracture mechanics studies. Such models require solid elements in the crack front region to capture strong through-thickness effects; modeling of the entire test specimen–structural element with solid elements then proves convenient. Unfortunately, the standard 8-node "brick" element with full integration exhibits strong shear-locking under bending deformations and thus overly stiff behavior. Three alternative elements are examined here: the 8-node element with single-point integration, the 8-node element with enhanced (incompatible) modes and the 20-node (quadratic) element. Element performance is assessed through analyses of a thin M(T) fracture specimen loaded in remote tension. This specimen generates strong compressive (T-)stresses parallel to the crack growth direction which leads to out-of-plane bending in the crack front region (triggered by a small normal force). The displacements obtained with a refined mesh of thin shell elements provide the reference solution for evaluation of the solid element performance. The analyses include large-displacement effects, but linear material response for simplicity, and are performed with Abaqus 5.6 and Warp3D. The results show clearly that both the 8-node element with enhanced modes and the 20-node element with conventional reduced integration provide solutions of accuracy comparable to the thin shell element. Mixed 8 and 20-node element meshes for ductile fracture analyses with transition elements to maintain displacement compatibility are demonstrated to provide an accurate and efficient modeling strategy.

1. Introduction

The finite element code WARP3D[1] for ductile fracture analyses provides an eight–node, solid element with full integration ($2 \times 2 \times 2$). Volumetric locking of the element under plastic deformation is minimized with the $\overline{B}$ formulation [2]. With refined meshes, this element has proven satisfactory for the modeling of conventional fracture specimens which have comparable dimensions in each direction. However, to capture the strong bending deformations present in thin shell–plate models, a large number (>8) of elements must be defined over the thickness. The "shear-locking" phenomenon resulting from the linear displacement field makes this element much too stiff in bending for thin shell applications.

This report describes a parametric study conducted to evaluate alternative 3-D solid elements for modeling ductile fracture in thin, shell-type specimens and structures. The alternative elements include: the 8-node brick with single point integration, the 8-node brick with enhanced modes, and the 20-node (quadratic) element with full and reduced integration. Three-dimensional crack extension models most often employ 8-node brick elements defined along the crack front and over the crack plane (linear displacement elements generally provide more robust models for very large deformations). To support a model constructed of 8-node elements at the crack front and 20-node elements elsewhere, a family of solid elements with 9 to15 nodes is described which facilitates transitioning between 8 and 20-node elements while maintaining displacement compatibility. A simple M(T) specimen is employed to evaluate the element performance. A small force applied normal to the plane of the specimen triggers out-of-plane bending in the crack front region. The naturally arising, compressive T-stress then amplifies the out-of-plane bending. Large displacement effects are included in the analyses but, for simplicity, the material remains linear elastic. Various levels of through-thickness mesh refinement are examined. A refined mesh of thin shell elements provides the reference solution for evaluation of the solid elements. All analyses are performed with Abaqus 5.6 [3] and Warp3D[1].

2. Thin Shell Fracture Model

2.1 Geometry

The structural component is a rectangular flat panel having dimensions of $20 \times 10 \times 0.05$ (in.) containing a horizontal centered crack of length $2a = 2$ in. (see Fig. 1). The component thus has a very large aspect ratio characteristic of "thin" shells. Symmetry conditions of the geometry and loading permit modelling of only one quarter of the panel.

2.2 Material

A linear elastic, isotropic constitutive model is adopted with properties assigned values typical of aluminum (Young's modulus = 15,000 ksi, Poisson ratio = 0.3).

2.3 Loading

The M(T) panel undergoes axial tension applied through a gradually imposed, remote displacement (Δ). The maximum value of this displacement is $\Delta/H = 0.0008$, which produces a nominal remote stress of $\sigma^{\infty} = 0.0008E$.

Due to the central crack, compression stresses develop parallel to the crack plane as illustrated in Fig. 2. Such stresses are generally referred to as T-stresses. These compression stresses may lead to local buckling or increase the out-of-plane displacements triggered by small

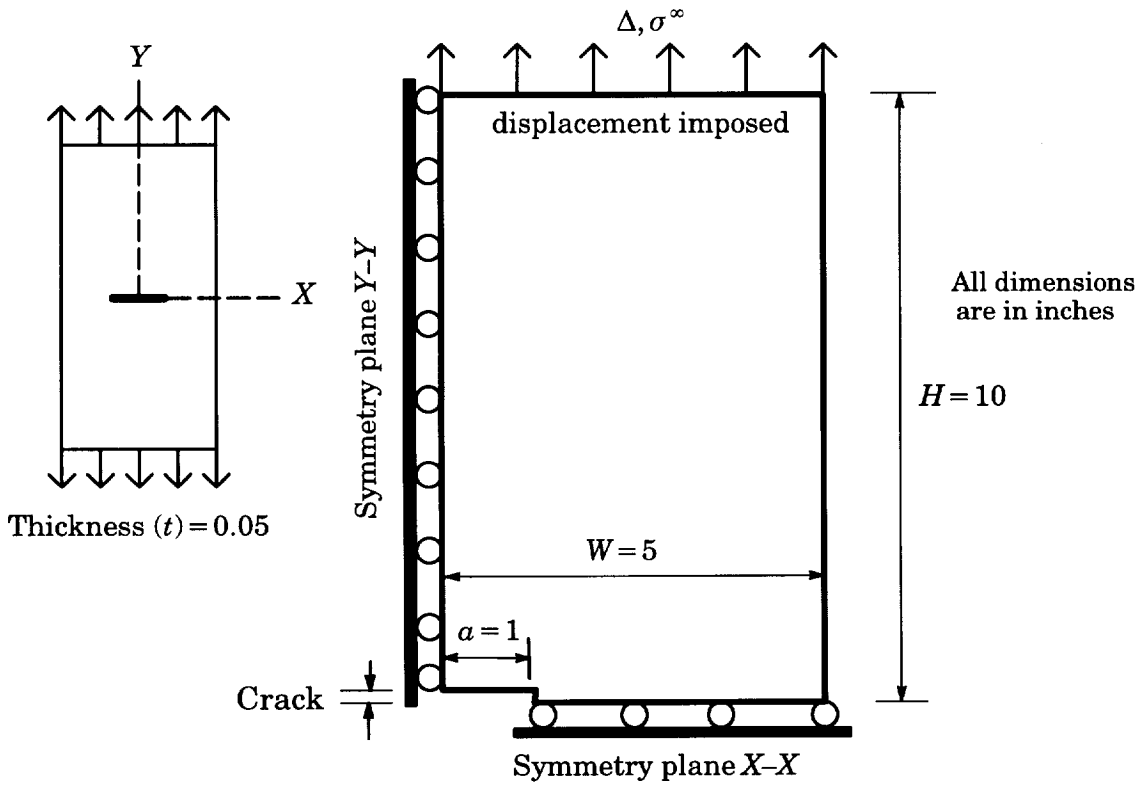

Figure 1. Quarter symmetric geometry of M(T) plate

imperfections. The finite element model contains no such imperfections. A small Z-direction concentrated force applied at the location $X=0$, $Y=0$ in the model triggers the out-of-plane displacement mode.

2.4 Boundary Conditions

The finite element model for the M(T) specimen has the following prescribed displacements.

Loading edge: $u=0, v=\Delta, w=0, \theta_x=0, \theta_y=0$ at $Y=0$.
Symmetry plane X–X: $v=0, \theta_x=0$ at $Y=0$.
Symmetry plane Y–Y: $u=0, \theta_y=0$ at $X=0$.

2.5 Finite Element Meshes

Two mesh designs, denoted coarse and fine, are defined for use in the parametric studies as shown in Fig. 3. In the X–Y plane, the coarse mesh has 200 elements per (thickness) layer while the fine mesh has 1683 elements per layer. In each case, refinement of the mesh focuses on the crack front region. In the Z–direction, the meshes incorporate 1, 2 or 4 layers of elements over the full thickness. The finite element meshes are generated using the PATRAN software.

3. Element Formulations

The shear locking phenomenon can be avoided by using elements with a quadratic displacement field, by reducing the order of integration (one less than full integration) or by introducing enhanced modes into linear displacement elements.

Except for the C3D8 element, each of the following solid elements incorporate in their formulation one of the above mentioned alternatives. The C3D8 element implements only the $\overline{B}$ formulation to reduce volumetric locking but otherwise has a linear displacement field. To maintain uniformity in the presentation, the ABAQUS names for these finite elements are retained.

C3D8 the 8-node solid finite element with a full integration, $\overline{B}$ formulation.

C3D8I the 8-node solid finite element including enhanced modes which improve the bending response. The element passes the patch test.

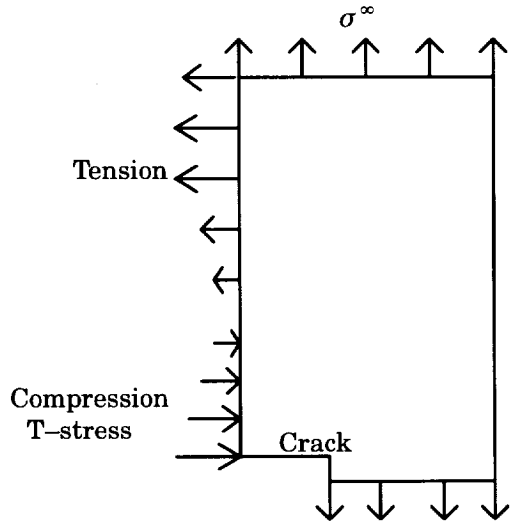

Figure 2. Qualitative distribution of boundary stresses

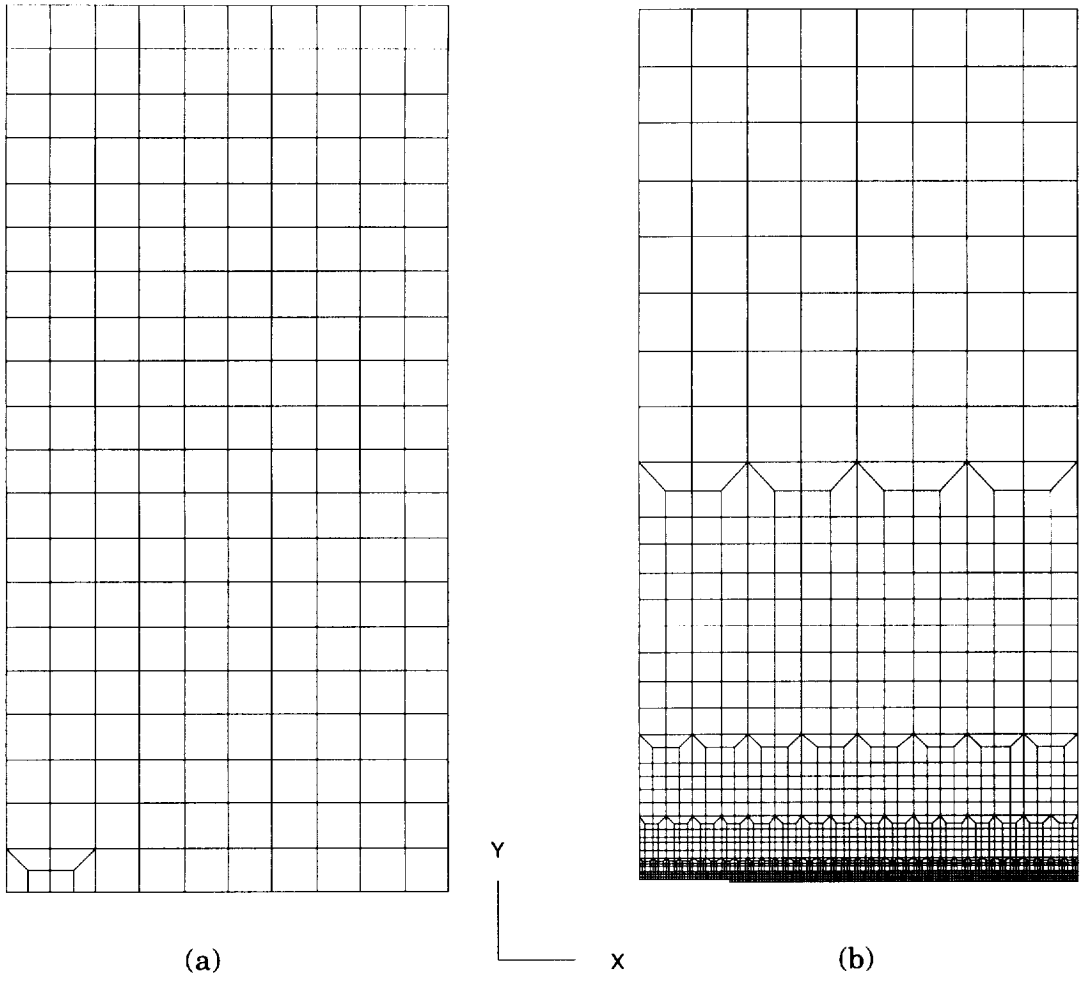

Figure 3. (a) Coarse mesh 200 elements/layer (b) Fine mesh 1683 elements/layer

C3D8R the 8-node solid finite element with 1 point integration and "hourglass" control.

C3D20 the 20-node solid finite element with full integration ($3 \times 3 \times 3$).

C3D20R the 20-node solid finite element with reduced integration ($2 \times 2 \times 2$).

The "reference" solutions for comparison are generated using the large displacement, shell element, S4R5.

4. Computational Procedures

The analyses are performed using the commercial finite element code, Abaqus Version 5.6. Abaqus 5.6 provides various shell elements that adequately model this problem and solid elements having options to improve bending response. The analyses use the NLGEOM option to include the effects of both large rotations and finite strains on the response. The sparse solver in Version 5.6 reduces the computational costs by at least a factor of 2 for these problems compared to the older wavefront solver.

4.1 Loading Cases

For each mesh and element type combination, three analyses are performed:

- a linear analysis with a small transverse load $P_z = P_S$
- a geometrically nonlinear analysis with a small transverse load $P_z = P_S$
- a geometrically nonlinear analysis with a large transverse load $P_z = P_L$

In the geometrically nonlinear analyses, the smaller triggering force, P_S, generates a maximum displacement at $X=0$, $Y=0$ of $0.8 \times t$, while the larger force, P_L, generates a maximum displacement of $2.5 \times t$. In all three cases, linear elastic material response is employed for simplicity.

4.2 Loading Process

The nonlinear analysis proceeds using a series of load increments within a single "step", in Abaqus terminology. In each load increment (i) both the displacement, Δ, imposed over the remote end and the transverse force, P_z, increase simultaneously as follows:

$$\Delta_i = \lambda_i \Delta$$

$$P_{z(i)} = \lambda_i P_z$$

where: $0 \le \lambda_i \le 1$, $\Sigma \lambda_i = 1$, $\Delta = 0.0008 \times H$ and $P_z = P_S$ or P_L.

Values of λ_i are specified to ABAQUS as: $\lambda_{1,2} = 0.05$, $\lambda_3 = 0.075$, $\lambda_{4-11} = 0.1$, and $\lambda_{12} = 0.025$. Equilibrium is attained after 2–4 Newton iterations for $P_z = P_S$ and 2–6 iterations for $P_z = P_L$.

5. Results and Discussion

This section describes the main results of the numerical analyses for the different elements and meshes. To determine the best solid finite element for use in modeling this type of thin shell component, three criteria are considered (in order of importance): (1) accuracy of model (reflected here by the computed displacements), (2) CPU time required, and (3) disk space required.

The first set of results compare the various 8–node and 20–node element solutions against the reference shell element solutions. The second set of results examines the response of models constructed using a mix of 8 and 20–node elements with 9–15 node elements employed to make the necessary transitions. These transition elements have been recently implemented in the Warp3D finite element code.

5.1 Global Behavior

Tables 1–3 summarize the computed out-of-plane displacements at $X=0$, $Y=0$ for each combination of mesh refinement and element type. The actual displacement values are provided in addition to the values normalized by the displacement of the shell element, fine mesh solution. Table 1 compares solutions for the linear elastic analysis. Tables 2 and 3 compare the geometrically nonlinear solutions for different levels of the applied, out-of-plane (triggering) force. As indicated in Tables 2 and 3, the smaller triggering force, P_S, generates a maximum displacement of $0.8 \times t$, while the larger force, P_L, generates a maximum displacement of $2.5 \times t$.

Figures 4–6 show the (magnified) deformed shapes for the linear and geometrically nonlinear analyses.

5.2 Summary of Element Performance

C3D8 This standard element is much too stiff; displacements are approximately 50% of shell solution values in each case. These results are not included in the tables.

C3D8I Good behavior but requires fine meshes. This element requires the minimum time and disk space of all solid elements. However, increasing the number of elements in thickness direction does not improve the solution. The solution thus never agrees with the shell element reference solution or the solution obtained using quadratic solid elements.

C3D8R Results are not good even for linear analysis. Accuracy degenerates severely in the nonlinear analyses. We did not attempt to "tune" the hourglass parameter for this model.

C3D20 Good results in all cases but computationally very expensive.

C3D20R Excellent agreement with shell solution, but computationally expensive for the fine mesh. However, the coarse mesh yields a very acceptable the solution.

S4R5 Used here to generate the reference solutions.

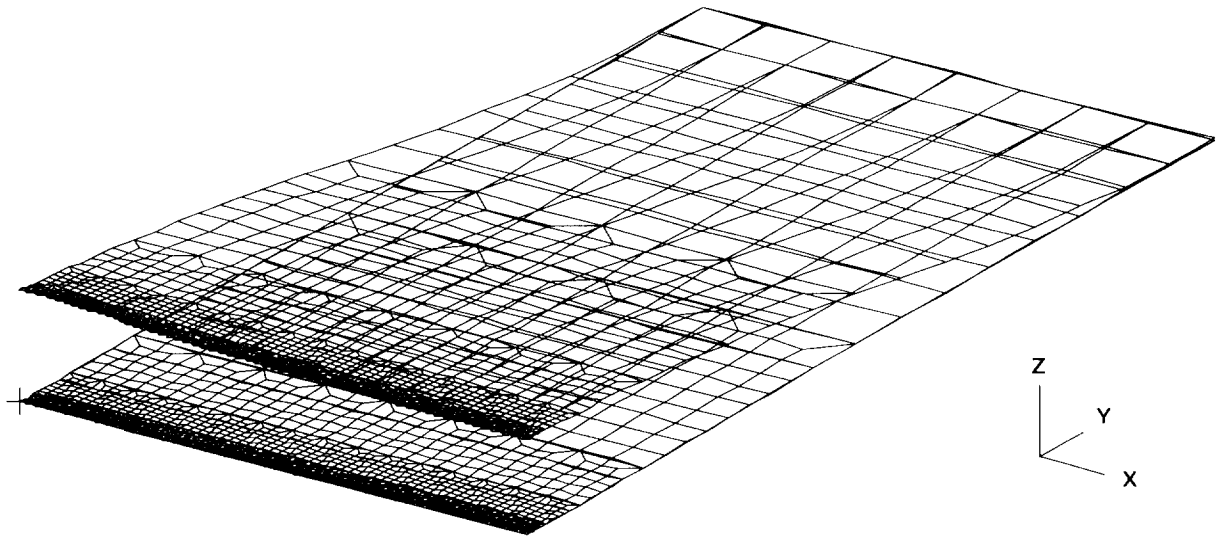

Figure 4. Deformed shape for linear analysis (shell elements)

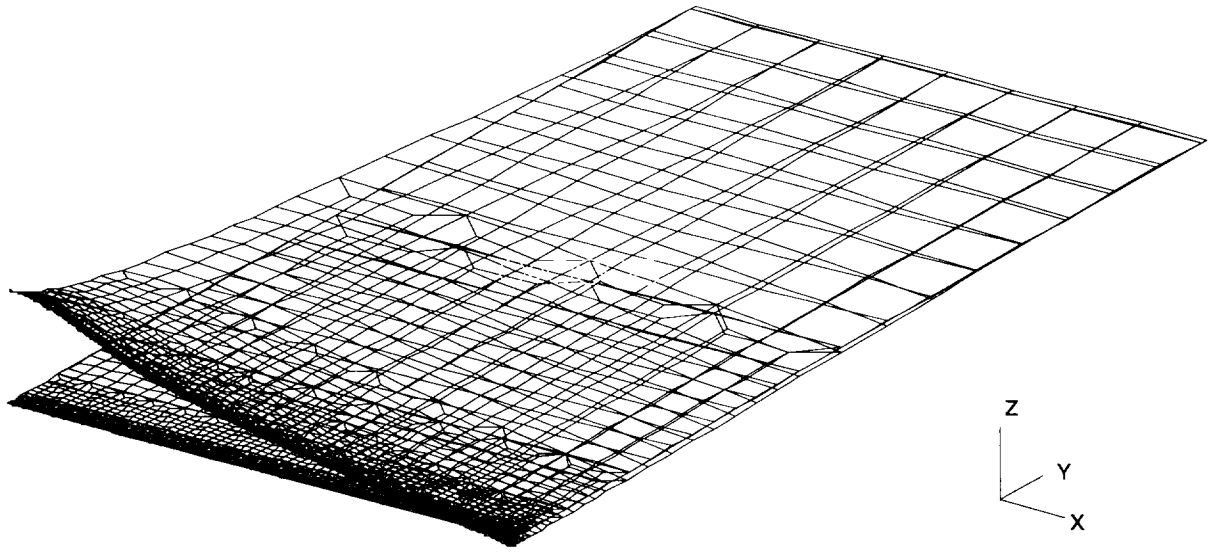

Figure 5. Deformed shape nonlinear analysis (shell elements)

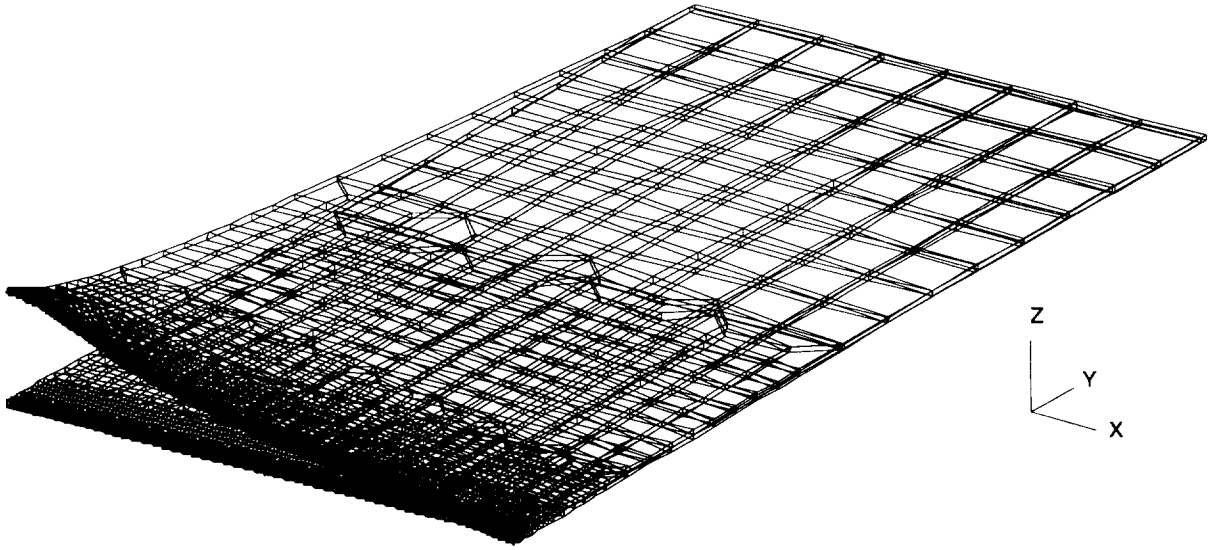

Figure 6. Deformed shape for nonlinear analysis (solid elements)

Mesh	Element	Type	w @ $X=0, Y=0$	
			(inches)	Normalized
Coarse	S4R5	shell	0.3913	0.986
	C3D8I (1 layer)	solid, enhanced modes	0.3525	0.888
	C3D8I (2 layers)	solid, enhanced modes	0.3501	0.882
	C3D8R (2 layers)	solid, hourglass	0.4399	1.108
	C3D8R (4 layers)	solid, hourglass	0.3493	0.880
	C3D20 (1 layer)	solid, full integration	0.3807	0.959
	C3D20R (1 layer)	solid, reduced integration	0.3921	0.988
Fine	S4R5	shell	0.3969	1.000
	C3D8I (1 layer)	solid, enhanced modes	0.3814	0.961
	C3D8I (2 layers)	solid, enhanced modes	0.3727	0.939
	C3D8R (2 layers)	solid, hourglass	0.4750	1.197
	C3D8R (4 layers)	solid, hourglass	0.3700	0.932
	C3D20 (1 layer)	solid, full integration	0.3920	0.988
	C3D20R (1 layer)	solid, reduced integration	0.3940	0.993
	C3D20R (2 layers)	solid, reduced integration	0.3965	0.999

Table 1. Linear Analysis ($P_z = P_S$)

Mesh	Element	Type	w @ $X=0, Y=0$		CPU Time
			(inches)	Normalized	
Coarse	S4R5	shell	0.0427	1.029	0.065
	C3D8I (1 layer)	solid, enhanced modes	0.0288	0.694	0.135
	C3D8I (2 layers)	solid, enhanced modes	0.0279	0.674	0.289
	C3D8R (2 layers)	solid, hourglass	0.0117	0.282	0.117
	C3D8R (4 layers)	solid, hourglass	0.0107	0.259	0.276
	C3D20 (1 layer)	solid, full integration	0.0364	0.876	0.646
	C3D20R (1 layer)	solid, reduced integration	0.0383	0.925	0.327
Fine	S4R5	shell	0.0415	1.000	1.000
	C3D8I (1 layer)	solid, enhanced modes	0.0390	0.939	2.162
	C3D8I (2 layers)	solid, enhanced modes	0.0389	0.939	5.552
	C3D8R (2 layers)	solid, hourglass	0.0261	0.630	2.230
	C3D8R (4 layers)	solid, hourglass	0.0190	0.457	6.821
	C3D20 (1 layer)	solid, full integration	0.0412	0.993	6.691
	C3D20R (1 layer)	solid, reduced integration	0.0414	0.999	4.159
	C3D20R (2 layers)	solid, reduced integration	0.0415	1.000	10.380

Table 2. Geometrically Nonlinear Analysis ($P_z = P_S$)

Mesh	Element	Type	w @ $X=0, Y=0$		CPU Time	Disk Space
			(inches)	Normalized		
Coarse	S4R5	shell	0.147	1.170	0.08	0.08
	C3D8I (1 layer)	solid, enhanced modes	0.097	0.773	0.15	0.13
	C3D8I (2 layers)	solid, enhanced modes	0.069	0.550	0.32	0.25
	C3D8R (2 layers)	solid, hourglass	0.044	0.353	0.12	0.12
	C3D8R (4 layers)	solid, hourglass	0.041	0.324	0.30	0.32
	C3D20 (1 layer)	solid, full integration	0.118	0.936	0.73	0.42
	C3D20R (1 layer)	solid, reduced integration	0.122	0.970	0.37	0.36
Fine	S4R5	shell	0.126	1.000	1.00	1.00
	C3D8I (1 layer)	solid, enhanced modes	0.122	0.967	2.28	1.63
	C3D8I (2 layers)	solid, enhanced modes	0.122	0.968	5.65	3.55
	C3D8R (2 layers)	solid, hourglass	0.094	0.750	2.38	1.82
	C3D8R (4 layers)	solid, hourglass	0.030	0.242	7.65	4.42
	C3D20 (1 layer)	solid, full integration	0.125	0.997	7.49	3.77
	C3D20R (1 layer)	solid, reduced integration	0.126	1.002	4.46	3.30
	C3D20R (2 layers)	solid, reduced integration	0.126	1.002	15.44	7.61

Table 3. Geometrically Nonlinear Analysis ($P_z = P_L$)

5.3 Response of Models with Solid Transition Elements

The above results clearly demonstrate the excellent bending behavior of the 20-node element with reduced integration ($2 \times 2 \times 2$). A single element defined over the thickness direction provides accurate solutions even with a relatively coarse, in-plane mesh. These promising results motivated implementation of the 20-node element and a family of transition elements with 9, 12, or 15 nodes in the Warp3D finite element code for modeling of ductile fracture. Fracture mechanics models for thin shell specimens and structural components analyzed with Warp3D may then employ the 8-node element over the initial crack front and along the anticipated growth plane. Elsewhere in the model, the adoption of 20-node elements provides excellent bending response. The various transition elements enable coupling of the 8 and 20-node elements with full displacement compatibility (see Fig. 7).

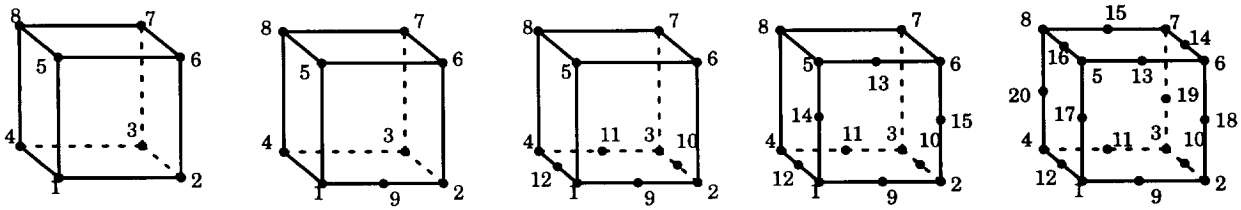

Figure 7. Warp3D solid elements

The family of 3-D solid elements in Warp3D for fracture mechanics modeling of thin shell structures includes:

l3disop 8-node linear displacement element, $2 \times 2 \times 2$ integration, $\overline{B}$ formulation.

q3disop 20-node element, $2 \times 2 \times 2$ integration.

t9isop 9-node transition element (1 edge is quadratic), $2 \times 2 \times 2$ integration.

t12isop 12-node transition element (1 face is quadratic), $2 \times 2 \times 2$ integration.

t15isop 15-node transition element (2 adjacent faces are quadratic), $2 \times 2 \times 2$ integration.

Two additional finite element models for the M(T) fracture specimen considered previously are constructed to evaluate the behavior of models containing these transition elements. The first model maintains the same in-plane layout as the fine mesh (1683 elements per layer) but uses 8-node elements in the neighborhood of the crack, 20-node elements elsewhere with a single strip of 12-node elements to make the transition. The model has two such layers in the thickness direction for a total of 3366 elements. The second mesh for comparison derives from the same fine mesh. However, the region of material to the right of the crack front is modeled with a much coarser mesh of 20-node elements (see Fig. 8). This model has two such layers defined over the thickness for a total of 2738 elements.

These models are analyzed for the same three conditions considered previously; (1) linear response with a small out-of-plane force, P_S; (2) large displacement analysis with the small out-of-plane force, P_S; and (3) large displacement analysis with the large out-of-plane force, P_L. Tables 4–6 summarize the computed displacements in the same format used previously. For comparison, the corresponding shell element and all 20-node element solutions are provided as well (generated with Abaqus). The meshes containing transition elements provide very high quality solutions with significant reductions in both CPU times and disk space (for restart files).

Code	Element(s)	Mesh	w @ $X=0, Y=0$	
			(inches)	Normalized
Abaqus	S4R5	1683 elements, 7053 nodes	0.3969	1.000
	C3D20R (2 layers)	3366 elements, 19000 nodes	0.3965	0.999
Warp3D	l3disop,t12,q3disop	3366 elements, 11690 nodes	0.4019	1.013
	l3d, t9, t12, t15, q3d	2738 elements, 10160 nodes	0.3951	0.995

Table 4. Linear Analysis ($P_z = P_S$)

Code	Element(s)	Mesh	w @ $X=0, Y=0$		CPU Time
			(inches)	Normalized	
Abaqus	S4R5	1683 elements, 7053 nodes	0.0415	1.000	1.000
	C3D20R (2 layers)	3366 elements, 19000 nodes	0.0415	1.000	10.380
Warp3D	l3disop,t12,q3disop	3366 elements, 11690 nodes	0.0411	0.990	3.520
	l3d, t9, t12, t15, q3d	2738 elements, 10160 nodes	0.0411	0.990	3.230

Table 5. Geometrically Nonlinear Analysis ($P_z = P_S$)

Code	Element(s)	Mesh	w @ $X=0, Y=0$		CPU Time	Disk Space
			(inches)	Normalized		
Abaqus	S4R5	1683 elements, 7053 nodes	0.1256	1.000	1.00	1.00
	C3D20R (2 layers)	3366 elements, 19000 nodes	0.1259	1.002	15.44	7.61
Warp3D	l3disop,t12,q3d	3366 elements, 11690 nodes	0.1251	0.992	4.32	3.25
	l3d, t9, t12, t15, q3d	2738 elements, 10160 nodes	0.1251	0.992	3.97	2.91

Table 6. Geometrically Nonlinear Analysis ($P_z = P_L$)

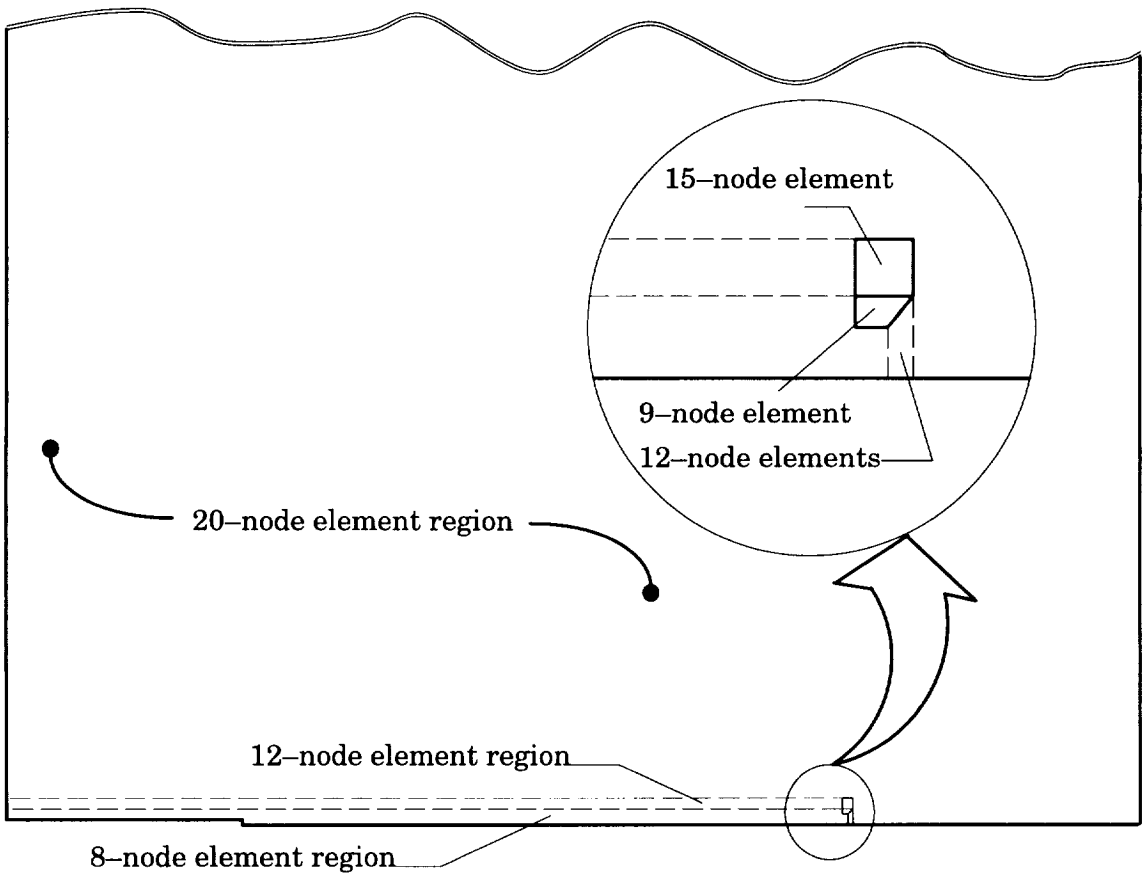

Figure 8. Distribution of finite elements (2 layers through thickness everywhere)

6. Concluding Remarks

This parametric study shows clearly that the 20-node (quadratic) element with reduced ($2 \times 2 \times 2$) integration provides the best combination of solution accuracy and computational cost to model bending in thin shell components for fracture mechanics studies. Accurate solutions may be obtained with a single layer of elements defined over the thickness coupled with

a relatively coarse in-plane mesh. The computed out-of-plane displacements, which are strongly sensitive to element performance in bending, agree very well with the reference solution obtained using thin shell elements.

The 8-node, linear displacement element with enhanced modes does provide a satisfactory solution, but only when the in-plane mesh has sufficient refinement. Not surprisingly, for a mesh with a fixed number of elements, the 20-node element yields superior solutions for these type models compared to the 8-node element with enhanced modes.

For modeling of ductile fracture in thin shells, the combination of 8-node elements (with $\bar{B}$) defined along the crack plane and 20-node elements elsewhere provides a robust, efficient modeling strategy. Transition elements maintain full displacement compatibility in such models. Solution accuracy essentially equals that of an all 20-node element model but with significant reduced CPU times and disk space requirements (for restart files).

Acknowledgements

Support for this study was provided by the NASA–Ames and NASA–Langley Research Centers under grants NCC2–5126 and NAG 2–1126.

References

1. Koppenhoefer, K., Gullerud, A., Ruggieri, C., Dodds, R. and Healy, B., "WARP3D: Dynamic Nonlinear Analysis of Solids Using a Preconditioned Conjugate Gradient Software Architecture", *Structural Research Series (SRS) 596*, UILU-ENG-94-2017, University of Illinois at Urbana-Champaign, 1994.

2. Hughes, T.J., Generalization of Selective Integration Procedures to Anisotropic and Nonlinear Media, *Int. J. Numer. Methods Eng.* 15 1413-1418 (1980).

3. Hibbitt, Karlsson, Sorensen. "ABAQUS/Standard User's Manual", Volume I, Version 5.6, HKS Inc., 1997.